Development 140, 2892-2903 (2013) doi:10.1242/dev.093229
© 2013. Published by The Company of Biologists Ltd

A replication-dependent passive mechanism modulates DNA demethylation in mouse primordial germ cells

Rika Ohno[1,*], Megumi Nakayama[1,*], Chie Naruse[2], Naoki Okashita[1,3], Osamu Takano[1], Makoto Tachibana[4], Masahide Asano[2], Mitinori Saitou[5,6,7,8,9] and Yoshiyuki Seki[1,3,5,‡]

SUMMARY

Germline cells reprogramme extensive epigenetic modifications to ensure the cellular totipotency of subsequent generations and to prevent the accumulation of epimutations. Notably, primordial germ cells (PGCs) erase genome-wide DNA methylation and H3K9 dimethylation marks in a stepwise manner during migration and gonadal periods. In this study, we profiled DNA and histone methylation on transposable elements during PGC development, and examined the role of DNA replication in DNA demethylation in gonadal PGCs. CpGs in short interspersed nuclear elements (SINEs) B1 and B2 were substantially demethylated in migrating PGCs, whereas CpGs in long interspersed nuclear elements (LINEs), such as LINE-1, were resistant to early demethylation. By contrast, CpGs in both LINE-1 and SINEs were rapidly demethylated in gonadal PGCs. Four major modifiers of DNA and histone methylation, *Dnmt3a*, *Dnmt3b*, *Glp* and *Uhrf1*, were actively repressed at distinct stages of PGC development. DNMT1 was localised at replication foci in nascent PGCs, whereas the efficiency of recruitment of DNMT1 into replication foci was severely impaired in gonadal PGCs. Hairpin bisulphite sequencing analysis showed that strand-specific hemi-methylated CpGs on LINE-1 were predominant in gonadal PGCs. Furthermore, DNA demethylation in SINEs and LINE-1 was impaired in *Cbx3*-deficient PGCs, indicating abnormalities in G1 to S phase progression. We propose that PGCs employ active and passive mechanisms for efficient and widespread erasure of genomic DNA methylation.

KEY WORDS: Primordial germ cells, PGCs, DNA demethylation, DNA replication, Epigenetic reprogramming

INTRODUCTION

In mammalian development, the fertilised oocyte generates diverse cell types that possess distinct gene expression profiles without changes in the primary sequence of the genome. These cell-specific transcriptional profiles are established and fixed in part through epigenetic mechanisms, including cytosine methylation and histone tail modification, which are mitotically heritable (Bird, 2002; Peters and Schübeler, 2005). By contrast, epigenetic modifications are extensively reprogrammed in early embryo and primordial germ cells (PGCs), the precursors of both oocytes and spermatozoa (Sasaki and Matsui, 2008). PGCs are specified from most proximal epiblast cells, accompanied by the induction of *Blimp1* (*Prdm1* – Mouse Genome Informatics) and *Prdm14* expression in mice (Ohinata et al., 2005; Yamaji et al., 2008). Subsequently, PGCs initiate migration towards future genital ridges through the hindgut and mesentery. Gonadal PGCs execute genome-wide demethylation, including erasure of parental imprints, to re-establish sex-specific imprints during subsequent gametogenesis (Hajkova et al., 2002). It has been shown that genome-wide epigenetic states of *Blimp1*-positive PGC precursors are indistinguishable from those of surrounding somatic cells at around embryonic day (E) 6.75 (Seki et al., 2007). Subsequently, PGCs erase global DNA methylation and histone H3 lysine 9 dimethylation (H3K9me2), after which H3K27me3 is induced throughout the genome during hindgut migration (Seki et al., 2005; Seki et al., 2007). Whole-mount immunofluorescence analysis using anti-5-methylcytosine antibody and locus-specific bisulphite sequencing analysis have provided evidence that DNA demethylation in PGCs occurs in a two-step manner during the migration and gonadal periods (Guibert et al., 2012; Seki et al., 2005). Recently, whole-genome bisulphite sequencing (BS-Seq) has elucidated the actual dynamics of global and locus-specific DNA methylation in developing PGCs (Kobayashi et al., 2013; Seisenberger et al., 2012). It has been suggested that genome-wide epigenetic reprogramming in PGCs plays an essential role in resetting epigenetic states, which are initially established during early embryogenesis, reacquiring cellular totipotency and preventing the accumulation of transgenerational epimutations.

DNA demethylation occurs through passive or active mechanisms. Passive DNA demethylation is triggered by the inhibition of the maintenance activity of DNA methyltransferases that accompany *de novo* DNA synthesis during DNA replication (Wu and Zhang, 2010). By contrast, active enzyme-catalysed DNA demethylation results in the removal of the methyl group from 5-methylcytosine (5mC) (Saitou et al., 2012). In plants, 5mC glycosylases and the base excision repair pathway are involved in active DNA demethylation (Zhu, 2009). Although mammalian homologues of 5mC glycosylases have not been identified, there is evidence that the base excision repair (BER) pathway modulates

[1]Department of Bioscience, School of Science and Technology, Kwansei Gakuin University, 2-1 Gakuen, Sanda, Hyogo 669-1337, Japan. [2]Division of Transgenic Animal Science, Kanazawa University, 13-1 Takara-machi, Kanazawa 920-8640, Japan. [3]Research Center for Environmental Bioscience, Kwansei Gakuin University, 2-1 Gakuen, Sanda, Hyogo 669-1337, Japan. [4]Experimental Research Center for Infectious Disease, Institute for Virus Research, Kyoto 606-8507, Japan. [5]Laboratory for Gem Cell Biology, Center for Developmental Biology, RIKEN Kobe Institute, 2-2-3 Minatojima-minamimachi, Chuo-ku, Kobe 650-0047, Japan. [6]Department of Anatomy and Cell Biology, Graduate School of Medicine, Kyoto University, Yoshida-Konoe-Cho, Sakyo-ku, Kyoto 606-8501, Japan. [7]Center for iPS Cell Research and Application, Kyoto University, 53 Kawahara-cho, Shogoin Yoshida, Sakyo-ku, Kyoto 606-8507, Japan. [8]JST, CREST/Exploratory Research for Advanced Technology (ERATO), Yoshida-Konoe-cho, Sakyo-ku, Kyoto 606-8501, Japan. [9]Institute for Integrated Cell-Material Sciences, Kyoto University, Yoshida-Ushinomiya-cho, Sakyo-ku, Kyoto 606-8501, Japan.

*These authors contributed equally to this work
‡Author for correspondence (yseki@kwansei.ac.jp)

Accepted 12 May 2013

active DNA demethylation in the paternal pronucleus (Gu et al., 2011; Hajkova et al., 2010; Iqbal et al., 2011; Wossidlo et al., 2011). Moreover, it has been reported that hydroxylation of 5mC to 5-hydroxymethylcytosine (5hmC), catalysed by ten eleven translocation (TET) proteins, is the first step of active DNA demethylation in the BER pathway in mammals (He et al., 2011; Ito et al., 2011). Although none of the 12 known human DNA glycosylases has been shown to act on 5hmC, 5-hydroxymethyluracil (5hmU), which is generated by the deamination of 5hmC by activation-induced cytosine deaminase (AID; AICDA – Human Gene Nomenclature Database), is the preferred target for DNA glycosylases, such as single-strand selective monofunctional uracil DNA glycosylase (SMUG1) and thymine DNA glycosylase (TDG) (Guo et al., 2011). AID-deficient PGCs have impaired global DNA demethylation and active markers of the BER pathway are transiently detected at E11.5 in developing PGCs, in which genome-wide epigenetic reprogramming occurs (Hajkova et al., 2010; Popp et al., 2010), suggesting that BER-mediated active DNA demethylation is involved in global DNA demethylation in developing PGCs. Because levels of DNA demethylation in AID-deficient PGCs are significantly lower than that in somatic cells, an alternative mechanism might exist for global DNA demethylation in the absence of AID functions (Popp et al., 2010). We have previously shown that several essential enzymes and modulators for DNA methylation and H3K9 methylation, including *Dnmt3a*, *Dnmt3b*, *Uhrf1* and *Glp* (*Ehmt1* – Mouse Genome Informatics), were specifically repressed in PGCs (Kurimoto et al., 2008; Seki et al., 2005; Seki et al., 2007; Yabuta et al., 2006). Considering these findings and the cell cycle dynamics of PGCs, we hypothesised that a passive mechanism modulated genome-wide epigenetic reprogramming in developing PGCs. In this article, to elucidate the molecular mechanisms for genome-wide epigenetic reprogramming in PGCs, we investigated the dynamics of epigenetic modifications in transposable elements. We found that CpG methylation was significantly decreased in migrating PGCs in short interspersed nuclear elements (SINEs), but not in long interspersed nuclear element-1 (LINE-1). By contrast, CpG methylation was efficiently demethylated in SINEs and LINE-1 in gonadal PGCs at ~E11.5. Hairpin bisulphite analysis, which defines DNA strand-specific CpG methylation, showed that the frequency of strand-biased hemimethylation in LINE-1 was gradually increased in PGCs between E9.5 and E11.5. Furthermore, DNA demethylation of transposable elements (TEs) was significantly disturbed in *Cbx3*-deficient PGCs, indicating an abnormality in the G1 to S phase transition (Abe et al., 2011). Our data demonstrated that rapid proliferation of PGCs accompanying active repression of *Uhrf1* and *Glp* promotes genome-wide DNA demethylation through a passive mechanism.

MATERIALS AND METHODS

Isolation of mouse embryos and purification of PGCs

All animals were treated with appropriate care according to the ethics guidelines of RIKEN, Kwansei-Gakuin University and Kanazawa University. Embryos were isolated in Dulbecco's modified Eagle's medium (Invitrogen) supplemented with 10% fetal calf serum (FCS; Stem Cell Science). At noon, when the vaginal plugs of mated females were identified, the score was recorded as E0.5. Embryonic fragments containing PGCs from *Dppa3*-EGFP or *Oct-3/4* ΔPE transgenic embryos at E8.5, E9.5, E10.5, E11.5 and E12.5 were dispersed into single cells by incubating with 0.25% trypsin, 0.5 mM EDTA in PBS. Enhanced green fluorescent protein (EGFP)-positive PGCs were sorted using a fluorescence-activated cell sorter, BD FACSAria (BD Bioscience) or JSAN (Bay Bioscience).

DNA methylation analysis

Bisulphite sequencing of PGCs was performed using a Methylamp Whole Cell Bisulphite Modification Kit (EPIGENTEK) following the manufacturer's conditions. For embryonic stem cells (ESCs), genomic DNA was isolated using the Wizard SV Genomic DNA Purification System (Promega), and bisulphite reactions were performed using a BisulFast DNA Modification Kit (TOYOBO), following the manufacturer's instructions. PCR primers used in this study are listed in supplementary material Table S1. PCR products were subcloned into the pGEM-T Easy vector (Promega) and sequenced.

Chromatin immunoprecipitation (ChIP) assay

ChIP assay was performed as previously described (Tachibana et al., 2008). For PGCs, we used 1000 cells per antibody as the starting material. The following antibodies were obtained from the indicated sources: rabbit anti-H3K9me1 (Upstate, 07-450), rabbit anti-H3K9me2 (Upstate, 07-212), rabbit anti-H3K9me3 (Upstate, 07-442), rabbit anti-H3K27me1 (Upstate, 07-448), rabbit anti-H3K27me2 (Upstate, 07-452), rabbit anti-H3K27me3 (Upstate, 07-449), rabbit anti-H3K4me2 (Upstate, 07-030), rabbit anti-H3K4me3 (Upstate, 07-473) and rabbit anti-H3 (Abcam, ab1791). For quantification of precipitated DNA, we performed real-time PCR analysis using the primers listed in supplementary material Table S1.

RNA expression analysis

Total RNA from PGCs and ESCs were extracted using RNeasy Micro Kit (QIAGEN) and Trizol (Invitrogen), respectively. ReverTra Ace qPCR RT Kit (TOYOBO) was used for cDNA synthesis, following the manufacturer's instructions. Subsequently, cDNA was used as template for RT-qPCR using a Thermal Cycler Dice Real Time System (TaKaRa) and Thunderbird SYBR qPCR Mix (TOYOBO) with gene-specific primers (supplementary material Table S1).

Whole-mount immunofluorescence analysis

Whole-mount immunofluorescence analysis was performed as previously described (Seki et al., 2005). The following antibodies were used at the indicated dilutions and obtained from specific sources: rabbit anti-DNMT1 (1/10, Santa Cruz Biotechnology, sc-20701); mouse anti-DNMT3A (1/300, Abcam, ab13888); mouse anti-DNMT3B (1/300, Abcam, ab13604); rat anti-GFP (1/500, Nacalai, 04404-84); mouse anti-PCNA (1/50, Santa Cruz Biotechnology, sc-56); rabbit anti-OCT-3/4 (1/300, Santa Cruz Biotechnology, sc-9081); and rat anti-UHRF1 (1/250, MBL, D289-3). The following secondary antibodies from Molecular Probes were used at 1/500: Alexa Fluor 488 goat anti-rat IgG, Alexa Fluor 488 goat anti-rabbit IgG, Alexa Fluor 568 goat anti-mouse IgG and Alexa Fluor 568 goat anti-rat IgG.

Cell culture

Dnmt-deficient ESCs were kindly provided by M. Okano of RIKEN CDB. *Uhrf1*-deficient ESCs were a generous gift from H. Koseki of RIKEN RCAI. Cells were cultured in feeder-free conditions in Glasgow Minimum Essential Medium (GMEM) (WAKO) containing 10% FCS (Invitrogen), 1 mM glutamine (WAKO), nonessential amino acids (WAKO) and 0.1 mM mercaptoethanol (WAKO), and supplemented with leukemia inhibitory factor (LIF; WAKO).

Hairpin bisulphite sequencing

Hairpin bisulphite sequencing analysis was carried out as described by Laird et al., with minor modifications (Laird et al., 2004). Genomic DNA was cleaved by *Bst*XI at 45°C overnight. Hairpin linkers were ligated to *Bst*XI-cleaved genomic DNA. The DNA was denatured in 0.6 M NaOH at 42°C for 20 minutes, followed by incubation at 100°C for 1 minute before the addition of a sodium bisulphite solution. The mixture was incubated at 99°C for 2 minutes and then at 55°C for 45 minutes, and this cycle was repeated six times. Subsequently, the mixture was purified by using a SV Gel and PCR Clean Up System (Promega), desulphonated with 0.3 M NaOH at 37°C for 20 minutes, and precipitated using ethanol. Bisulphite DNA was amplified using the primers listed in supplementary material Table S1. The PCR products were subcloned into the pGEM-T Easy vector (Promega) and sequenced.

RESULTS

DNA methylation profiling of TEs in developing PGCs

We previously demonstrated dynamic changes in genome-wide epigenetic modifications associated with G2 cell cycle phase arrest during early PGC development (Seki et al., 2005; Seki et al., 2007) (Fig. 1A). Whole-mount immunofluoresence analysis using a 5mC antibody showed that global levels of DNA methylation were reduced in a two-step manner during PGC development (Seki et al., 2005). Interspersed repeats, such as SINEs B1 and B2 and LINEs (LINE-1), are integrated across the entire mouse genome (Fig. 1B), and CpG sites on these interspersed repeats are heavily methylated in somatic cells. Considering these facts, we focused on DNA methylation of TEs because the reduction in 5mC immunofluorescence signals might reflect the loss of DNA methylation on TEs in PGC development. We monitored the CpG

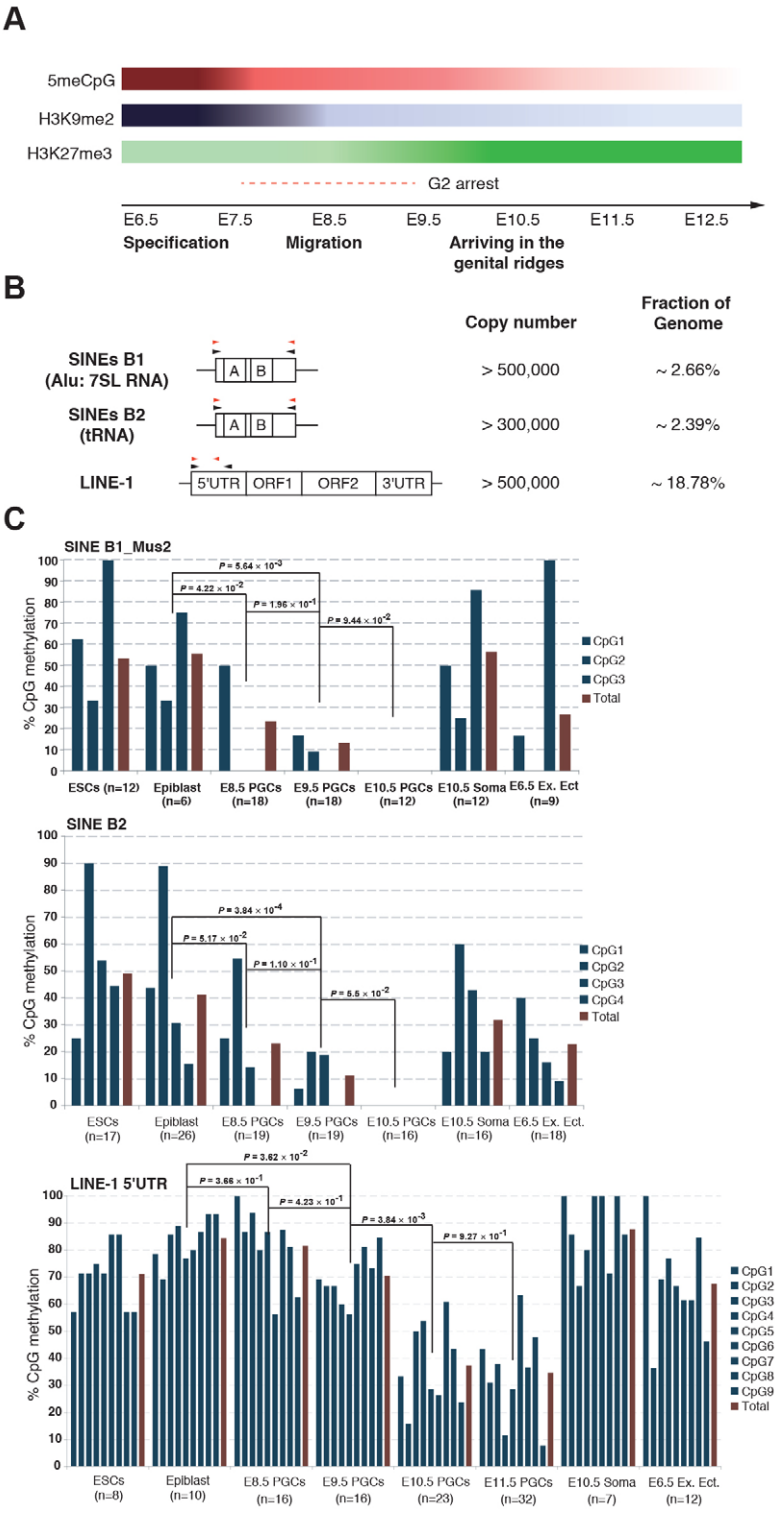

Fig. 1. Distinct dynamics of CpG methylation on transposable elements in PGCs. (**A**) Schematic of the dynamics of genome-wide epigenetic modifications and cell cycle status in developing PGCs. (**B**) The distribution of transposable elements in the mouse genome. Specific primers are indicated: black arrowheads represent bisulphite sequencing primer and red arrowheads represent ChIP primer. (**C**) Bisulphite sequencing analysis of transposable elements in ESCs, epiblast cells, PGCs, somatic cells and extra-embryonic ectoderm cells. Blue bar shows average percentage of methylation at individual CpG sites; red bar shows average percentage of methylation on total CpG sites. *P* values for bisulphite sequencing were obtained using the non-parametric two-tailed Mann–Whitney *U* test.

methylation status of SINEs and LINE-1 in developing PGCs isolated by cell sorting of *Dppa3*-EGFP-positive cells (Payer et al., 2006). Bisulphite sequencing analysis clearly demonstrated distinct dynamics of CpG methylation of SINEs and LINE-1 during PGC differentiation (Fig. 1C). DNA methylation of SINE B1, except on CpG1, was completely erased in PGCs until E8.5, when PGCs had just entered the embryo proper from the extra-embryonic mesoderm. The levels of SINE B2 CpG methylation were gradually reduced in PGCs at E8.5-E9.5. By contrast, CpG methylation of LINE-1 was resistant to DNA demethylation mechanisms that occur in migrating PGCs. DNA methylation levels in SINEs and LINE-1 were abruptly decreased in PGCs between E9.5 and E10.5, during which time PGCs rapidly re-proliferate (Fig. 1C) (Seki et al., 2007). These results raised the possibility that two distinct molecular mechanisms of DNA demethylation exist in PGCs in the migration (~E6.5-E8.5) and gonadal (~E9.5) periods.

Histone methylation profiling of TEs in developing PGCs

DNA methylation is closely linked to H3K9 methylation (Dong et al., 2008; Tachibana et al., 2008), and we have previously shown that migrating PGCs erase and increase genome-wide H3K9me2 and H3K27me3 marks, respectively (Seki et al., 2005; Seki et al., 2007). We also performed ChIP analysis for major histone methylations, namely H3K4, H3K9 and H3K27, on TEs in epiblast cells, PGCs and somatic cells. Although the small amount of sample obtained from PGCs made it difficult to carry out ChIP analysis, SINEs and LINE-1 were widely distributed throughout the mouse genome (Fig. 1B), and our SINEs and LINE-1 ChIP primer sets were detected in ~1000-10,000 copies of these elements in developing PGCs (supplementary material Fig. S1). To establish positive controls for ChIP analysis by using anti-H3K9me2, -H3K27me1/H3K27me3, -H3K27me3 and -H3K4me2/3 antibodies, we first analysed ESCs using primer sets against *Magea2*, major satellite, *Hoxb1* and *Oct-3/4* (*Pou5f1* – Mouse Genome Informatics), respectively (supplementary material Fig. S2) (Agger et al., 2007; Feldman et al., 2006; Martens et al., 2005; Tachibana et al., 2002). We applied the precipitation efficiency of our positive control against each antibody to evaluate the enrichment of each histone methylation. According to these criteria, in epiblast cells, which are a source of both PGCs and somatic cells, H3K9me2 was enriched in SINEs and LINE-1 (Fig. 2A), and H3K9me2 in TEs consistently increased during differentiation from epiblast cells to somatic cells. By contrast, we found that H3K9me2 was significantly reduced in SINEs and slightly but non-significantly reduced in LINE-1 elements in PGCs compared with those in epiblast cells. Moreover, H3K27me1 levels in TEs were reduced in PGCs between E9.5 and E11.5, whereas the H3K27me2/3 levels in TEs were relatively increased in developing PGCs. Furthermore, H3K4me3 levels were consistently reduced on SINEs and LINE-1 in somatic cells but not in developing PGCs. Collectively, these results demonstrated that repressive modifications of TEs, namely DNA methylation and H3K9 dimethylation, are reprogrammed in an orderly manner during early PGC development (Fig. 2B). We proceeded to analyse whether dynamic epigenetic modifications of TEs affect transcriptional activity. Surprisingly, DNA methylation and H3K9me2 on SINEs were completely absent in gonadal PGCs, whereas the transcription levels of SINEs were relatively comparable to those in surrounding somatic cells. By contrast, the expression of LINE-1 was significantly increased in step with the reduction in the DNA methylation of LINE-1 5′UTR in gonadal PGCs (Fig. 2C).

Active repression of GLP might be involved in the demethylation of H3K9me1/2 in developing PGCs

We previously showed that GLP, a critical component of protein complexes regulating H3K9 methylation, is repressed in migrating PGCs at E7.75 (supplementary material Fig. S3) (Seki et al., 2007). To determine whether GLP participates in H3K9 dimethylation in SINEs and LINE-1, we compared the levels of TE histone methylation in wild-type and *Glp*-deficient ESCs. The levels of H3K9me1/2 in SINEs were consistently decreased in *Glp*-deficient ESCs. Although we also found a slight reduction of H3K9me1/2 levels on LINE-1, H3K9me2 was still enriched in LINE-1 in *Glp* knockout (KO) ESCs, suggesting that GLP and another enzyme cooperate to confer H3K9me2 on LINE-1 in ESCs, a fact consistent with a slight reduction of H3K9me2 in LINE-1 in developing PGCs. Abrogation of G9a, an essential partner of GLP for H3K9 mono- and dimethylation, is associated with a significant reduction in DNA methylation in ESCs of long terminal repeat (LTR) transposons, intracisternal A particle (IAP) and major satellite repeats, but not of LINE-1 (Dong et al., 2008). Moreover, consistent with previous reports, CpG methylation levels of SINEs and LINE-1 are maintained in *Glp*-deficient ESCs (Fig. 3B). Collectively, these findings suggest that active repression of GLP results in a reduction of H3K9me1/2 in SINEs and LINE-1 in migrating PGCs.

Loading of DNMT1 at replication foci is disturbed in late but not early PGCs

We previously showed that nascent PGCs proliferate rapidly until E7.25, after which time the majority of PGCs enter transient G2 cell cycle arrest from E7.75 to E8.75 (Fig. 1A) (Seki et al., 2007). The timing of genome-wide DNA demethylation in PGCs during the migration and gonadal periods is consistent with the stages in which PGCs undergo active proliferation. Although whole-mount immunofluorescence analysis showed that DNMT1 was consistently expressed in developing PGCs, we did not observe punctate localisation of DNMT1, which represents the recruitment of DNMT1 to replication foci, in PGCs at E10.5 (supplementary material Fig. S3A). Our single-cell microarray analysis showed that the expression of *Uhrf1*, a guidance factor involved in the loading of DNMT1 at replication sites (Sharif et al., 2007), was specifically repressed in PGCs after E7.5 (Kurimoto et al., 2008). To determine whether specific repression of *Uhrf1* was maintained during PGC development, we analysed the mRNA levels of *Uhrf1* in epiblast cells, PGCs and somatic cells by qRT-PCR. Consistently low levels of *Uhrf1* expression were observed in developing PGCs until E11.5 (Fig. 4A). To monitor the UHRF1 protein levels in PGCs, we performed whole-mount immunofluorescence analysis using an anti-UHRF1 antibody. *Prdm1*-mVENUS transgenic embryos were used to visualise the nascent PGCs using membrane-targeted VENUS (Ohinata et al., 2005); non-transgenic embryos stained using an anti-OCT4 antibody were used to visualise migrating and gonadal PGCs (Yamaji et al., 2008). Germ cells weakly positive for *Prdm1* retained UHRF1 expression as seen in the surrounding somatic cells, whereas UHRF1 expression was slightly reduced in germ cells strongly positive for *Prdm1*, and it was subsequently completely lost in developing PGCs between E8.5 and E11.5 (Fig. 3B). In the middle of S phase of the cell cycle, the site of DNA synthesis can be visualised by PCNA in pericentric heterochromatin together with dense Hoechst staining

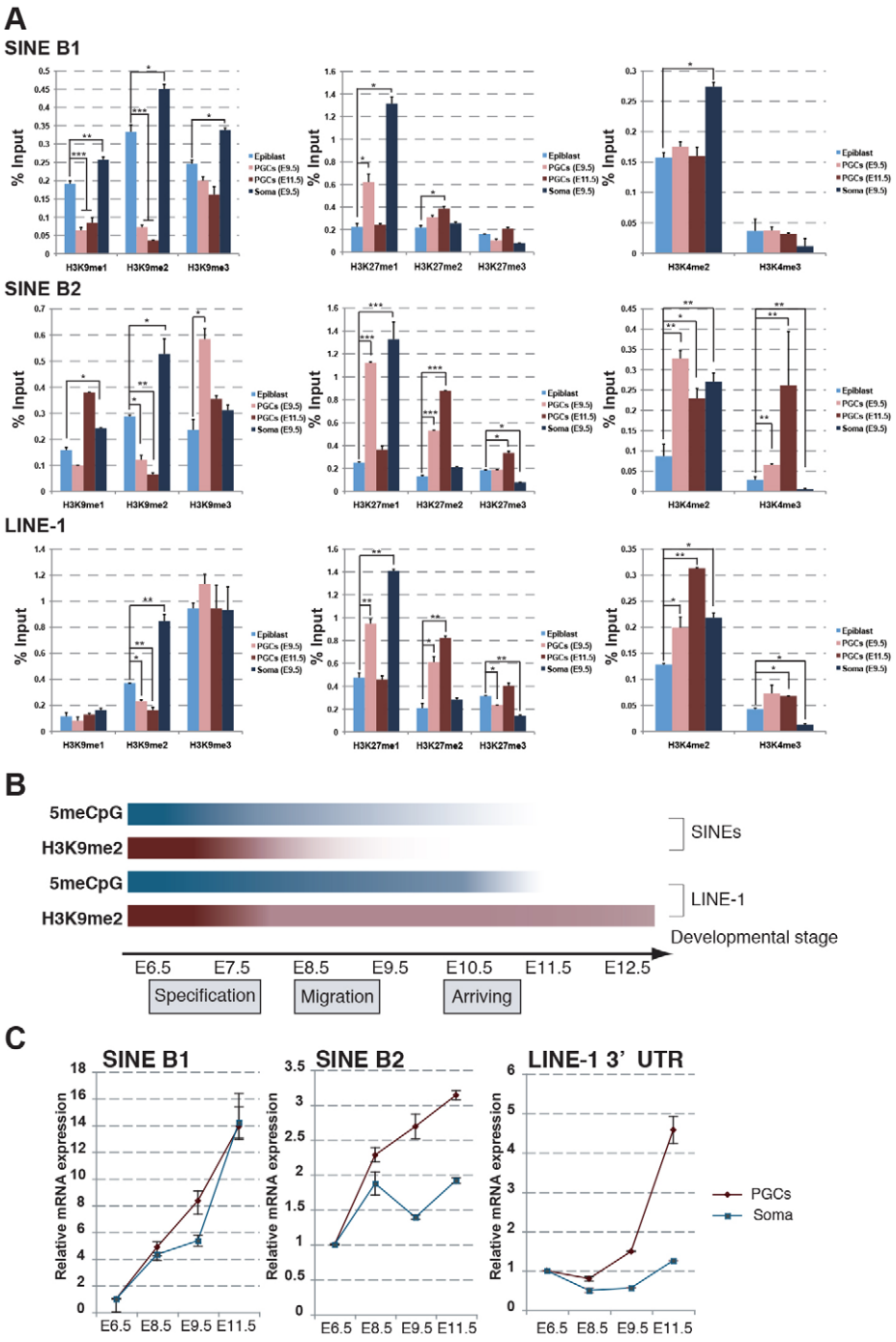

Fig. 2. H3K9, H3K27 and H3K4 methylation profiles in transposable elements of ESCs, epiblast cells, PGCs and somatic cells. (**A**) ChIP-qPCR analysis of transposable elements. Control experiments against each antibody are shown in supplementary material Fig. S3. The *y*-axis shows percentage of input recovery; error bars represent s.e.m. from two technical replicates of qPCR. (**B**) Schematic overview of epigenetic reprogramming on transposable elements in PGCs. (**C**) Expression of transposable elements in epiblast cells, PGCs and somatic cells. Expression levels in epiblasts are set as 1. *P* values for ChIP and qRT-PCR were obtained using Student's *t*-test. **P*<0.05, ***P*<0.01, ****P*<0.001.

(supplementary material Fig. S4). Consistent with previous reports, DNMT1 accumulated in the replicating pericentric heterochromatin region in wild-type ESCs, but little or no enrichment of DNMT1 was observed in the replicating pericentric heterochromatin regions in *Uhrf1*-deficient ESCs (Sharif et al., 2007). To examine whether the loss of UHRF1 expression disturbed the accumulation of DNMT1 in replicating heterochromatic regions in developing PGCs, we analysed the nuclear distribution of DNMT1 by whole-mount immunofluorescence analysis with anti-GFP, -DNMT1 and -PCNA antibodies in *Prdm1*-mVENUS and *Dppa3*-EGFP transgenic embryos. At the late-streak (LS) stage (E6.75) and the mid-bud (MB) stage (E7.5), when PGCs proliferate rapidly (first proliferation phase) prior to entering G2 cell cycle arrest (Seki et al., 2007), we observed significant accumulation of DNMT1 at DNA synthesis sites in the middle of S phase in PGCs (Fig. 4B). The expression of UHRF1 was low in migrating PGCs until E8.5; however, the majority of migrating PGCs entered G2 cell cycle arrest, which suggests that passive demethylation does not occur in migrating PGCs. Our previous study showed that PGCs re-proliferate rapidly (second proliferation phase) after E9.5 (Seki et al., 2007). At the second proliferation phase of PGCs, DNMT1 exhibited a diffuse localisation pattern in PGCs at E9.5 and E10.5 (Fig. 4B). In concert, these findings suggest that the specific

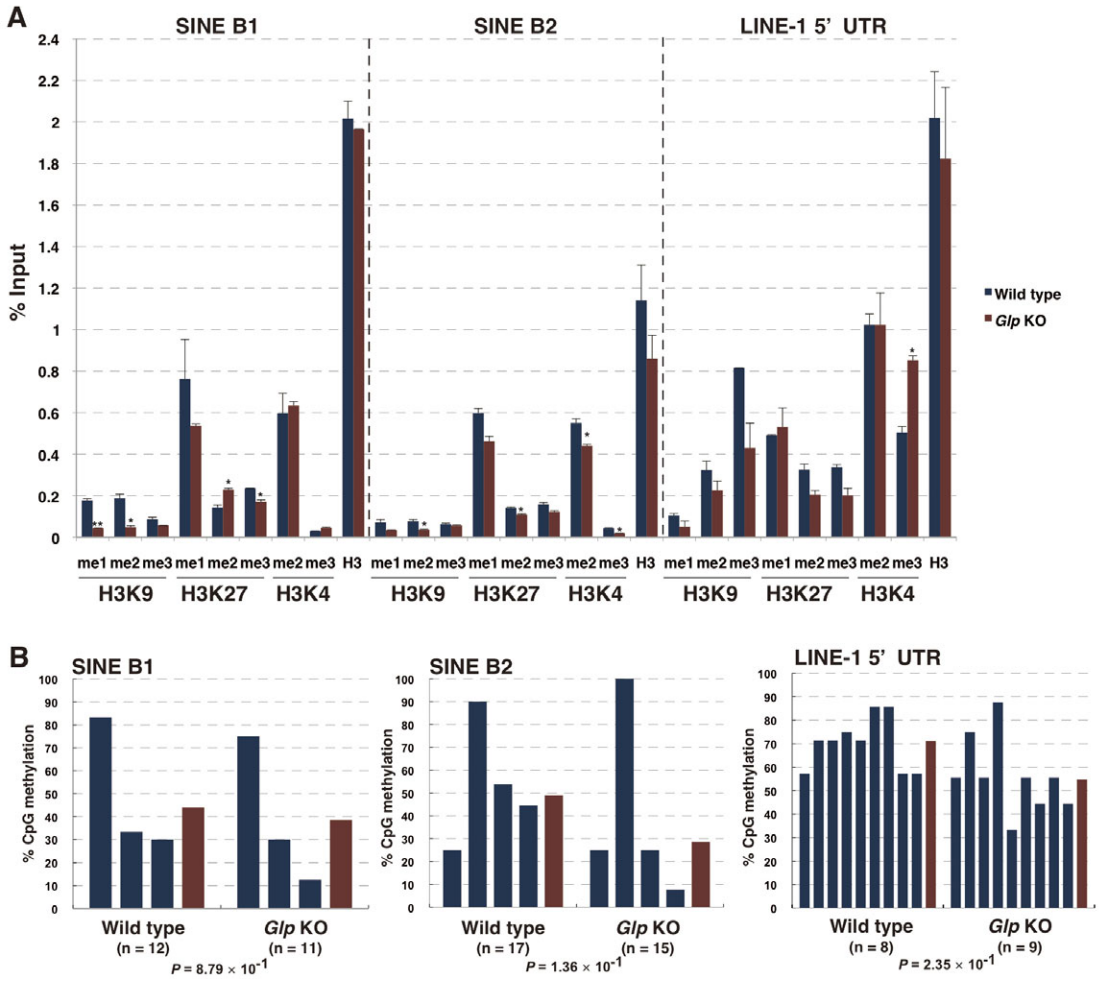

Fig. 3. Histone and DNA methylation profiles in transposable elements in *Glp* KO ESCs. (**A**) ChIP-qPCR analysis of transposable elements in wild-type and *Glp* KO ESCs. The *y*-axis shows percentage of input recovery; error bars represent s.e.m. from two technical replicates of qPCR. (**B**) Bisulphite sequencing analysis of transposable elements in wild-type and *Glp* KO ESCs. Blue bar shows average percentage of methylation at individual CpG sites; red bar shows average percentage of methylation on total CpG sites. *P* values for ChIP and qRT-PCR were obtained using Student's *t*-test. **P*<0.05, ***P*<0.01. *P* values for bisulphite sequencing were obtained using the non-parametric two-tailed Mann–Whitney *U* test.

repression of UHRF1 disrupts the loading of DNMT1 at PGC replication sites after E9.5.

High frequency of strand-biased LINE-1 hemimethylation in developing PGCs

Because disruption of DNMT1 loading at the replication site was anticipated to result in strand-biased hemimethylation of CpG sites, we monitored the hemimethylation status of LINE-1 using hairpin bisulphite sequencing analysis, which indicates the extent of methylation symmetry between complementary DNA strands (Fig. 5A,B) (Laird et al., 2004). Consistent with previous reports, the total methylation rate of CpG sites on LINE-1 was decreased in *Uhrf1*-deficient ESCs (Fig. 5C,D) (Sharif et al., 2007). Unexpectedly, we observed a relatively high frequency (22.3%) of LINE-1 CpG hemimethylation in wild-type ESCs. This observation suggested that the maintenance error of CpG methylation on LINE-1 during DNA replication often occurs in the cultivation of wild-type ESCs, which was consistent with a recent study (Arand et al., 2012). The frequency of hemimethylated LINE-1 CpG sites was significantly increased in *Uhrf1*-deficient ESCs (Fig. 5E). In the case of passive DNA demethylation associated with DNA replication, maintenance methylation of newly synthesised CpG sites does not occur, resulting in strand-biased hemimethylation of LINE-1. Therefore, we compared the frequency of strand-biased and unbiased hemimethylated clones in wild-type and *Uhrf1*-deficient ESCs. We found a high frequency of strand-biased hemimethylated clones of LINE-1 in *Uhrf1*-deficient ESCs compared with those in wild-type ESCs (Fig. 5F). In *Uhrf1*-deficient ESCs, the frequency of fully methylated clones on LINE-1 decreased with the elevation of frequency of non-methylated clones on LINE-1. These results provide evidence that hairpin bisulphite sequencing analysis can monitor the appearance of strand-biased hemimethylation accompanying the loss of *Uhrf1* in ESCs.

We next applied hairpin bisulphite sequencing analysis of LINE-1 in developing PGCs. Because PGCs are specified from the most proximal epiblast cells at ~E6.0-E6.75, we first monitored hemimethylation of CpG sites of LINE-1 in epiblast cells at the LS stage (E6.75). In epiblast cells, CpG sites on LINE-1 were heavily methylated and the frequency of strand-biased hemimethylated clones was low (Fig. 6A-C). LINE-1 CpG methylation patterns in somatic cells were similar to those in epiblast cells. In the case of

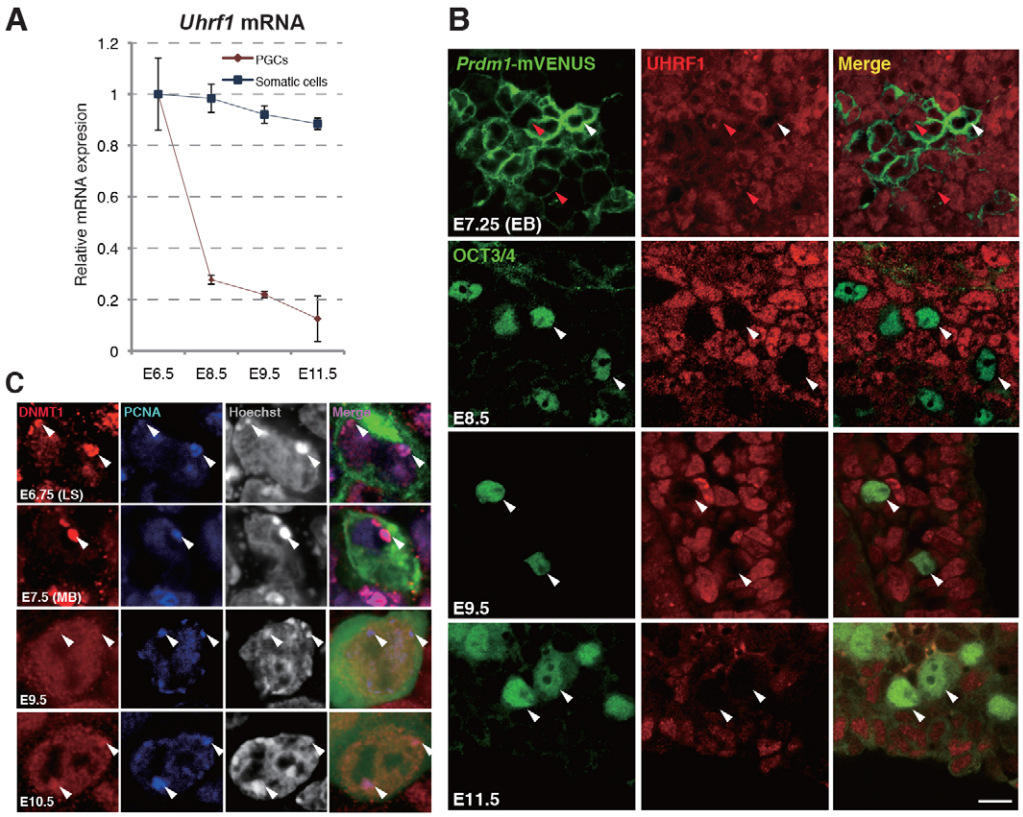

Fig. 4. Recruitment of DNMT1 into replication foci is impaired in gonadal PGCs. (**A**) qRT-PCR analysis of *Uhrf1* using cDNA derived from epiblasts (E6.5) and PGCs (E8.5, E9.5, E11.5). Error bars represent the s.e.m. from two technical replicates of qPCR. (**B**) Expression of UHRF1 in *Prdm1*-positive nascent PGCs (green) and OCT-3/4 (green)-positive in migrating and gonadal PGCs. Red arrowheads indicate weakly *Prdm1*-positive PGCs with UHRF1 expression. White arrowheads indicate strongly *Prdm1*-positive and OCT-3/4-positive PGCs with repressed UHRF1. Scale bar: 10 μm. (**C**) Nuclear localisation of DNMT1 in the middle of S phase of the cycle. Arrowheads indicate replication foci with a PCNA- and Hoechst-dense region.

PGCs, the percentage of total CpG methylation was decreased, accompanying the elevation of the percentage of total CpG hemimethylation in gonadal PGCs from E10.5 to E11.5 (Fig. 6B). In particular, the frequency of strand-biased hemimethylated clones in PGCs was significantly elevated from E10.5 to E11.5, raising the possibility that the maintenance of CpG methylation of LINE-1 was disturbed in PGCs from E10.5 to E11.5 (Fig. 6C).

Abnormalities in global DNA demethylation in *Cbx3*-deficient PGCs

We have previously shown that the loss of *Cbx3* severely impairs G1 to S phase progression in developing PGCs (Abe et al., 2011). To determine whether the rapid proliferation of PGCs is involved in global DNA demethylation, we compared the DNA methylation states of TEs and imprinted loci in wild-type and *Cbx3*-deficient PGCs at E11.5. Consistent with the data shown in Fig. 1C, SINE B1 and B2 CpG methylation was undetectable in wild-type PGCs at E11.5. Interestingly, *Cbx3*-deficient PGCs had substantially higher levels of SINE B1 and B2 CpG methylation than did wild-type PGCs. DNA methylation levels of both SINE B1 and B2 in *Cbx3*-deficient PGCs were comparable to those in epiblast cells (Fig. 1C; Fig. 7A), clearly indicating that the erasure of SINE DNA methylation is severely impaired in *Cbx3*-deficient PGCs. The impairment of DNA demethylation in *Cbx3*-deficient PGCs was also observed in LINE-1. By contrast, the erasure of genomic imprints was normal in *Cbx3*-deficient PGCs (Fig. 7B).

DISCUSSION

Global DNA demethylation in migrating PGCs

Here, we have carried out the first comprehensive analysis of DNA and histone methylation profiles on TEs in developing PGCs. Our previous whole-mount immunofluorescence analysis showed that global DNA demethylation occurred at two distinct stages in PGC development during migration and gonadal periods (Seki et al., 2005). Until recently, although the DNA methylation status of imprinted loci and TEs in gonadal PGCs has been extensively analysed (Guibert et al., 2012; Hajkova et al., 2002; Popp et al., 2010), DNA methylation analysis in migrating PGCs has been limited to immunostaining with an antibody against 5mC, and genomic sequences targeted for demethylation in migrating PGCs have not been identified. A recent report uncovered a global DNA demethylation in migrating PGCs by whole-genome bisulphite sequencing analysis up to E9.5 (Seisenberger et al., 2012). Consistent with this study, our results clearly demonstrate that CpG methylation in SINEs are targets for global DNA demethylation in migrating PGCs. Furthermore, our data confirm that significant reduction of CpG methylation in SINEs occurs in migrating PGCs up to E8.5, which is consistent with our previous immunofluorescence analysis and bisulphite analysis of individual loci (Guibert et al., 2012; Seki et al., 2005). The current study, as well as our previous study, strongly supports the idea that global DNA demethylation takes place in migrating PGCs until E8.5.

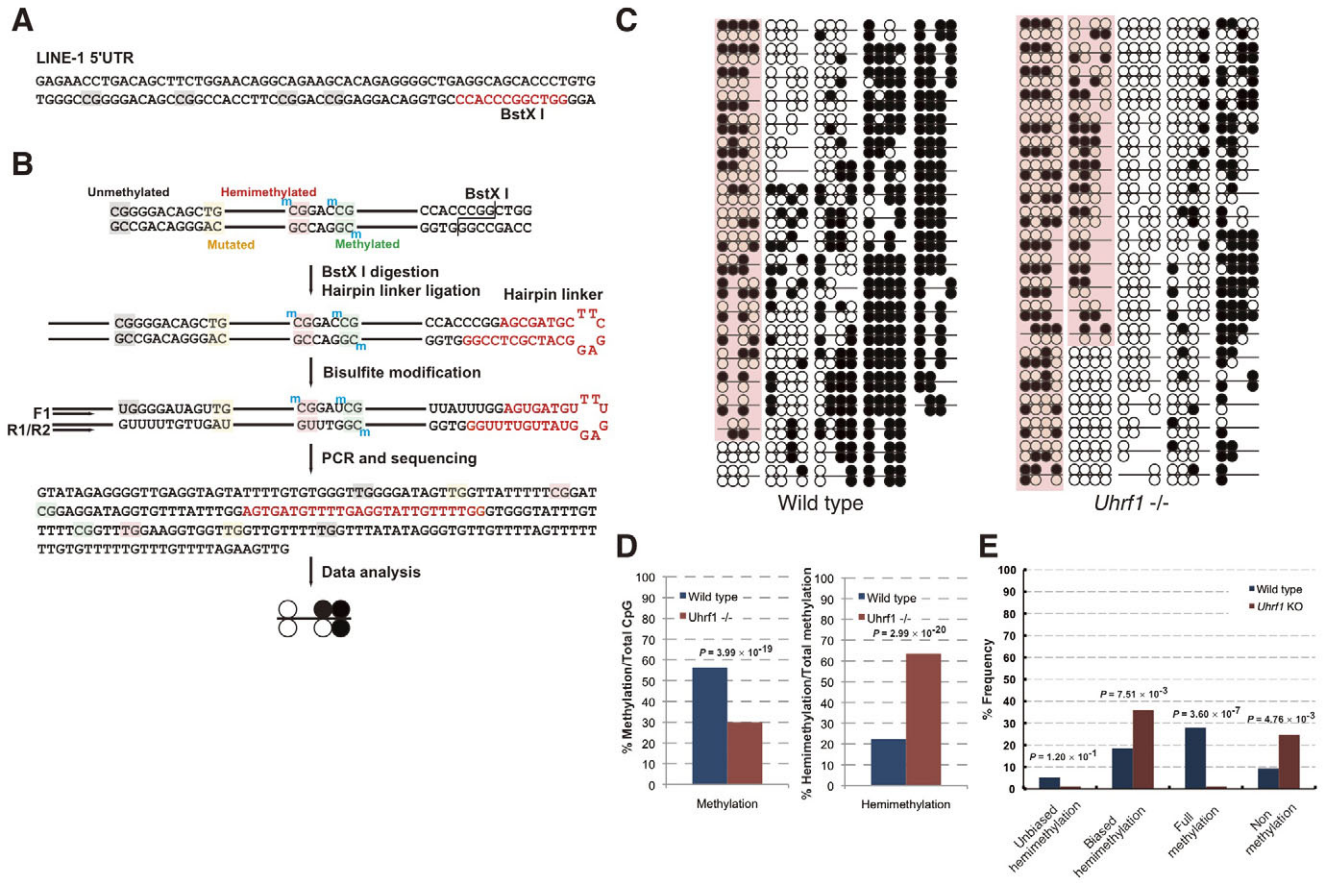

Fig. 5. Hairpin bisulphite sequencing monitors hemimethylation by loss of UHRF1. (**A**) Conserved sequence of LINE-1 5′UTR and the position of the recognition sequence of *Bst*XI. (**B**) Schematic of hairpin bisulphite sequencing. ^{m}C indicates 5-methylcytosine. Upper and lower strands are ligated by a hairpin linker followed by bisulphite treatment. F1 and R1/R2 indicate the position of semi-nested PCR primers. (**C**) Methylation patterns are represented by circles. Filled, methylated; open, unmethylated. Pink shading indicates biased hemimethylated clones as described below. (**D**) The total amount of methylated CpGs per total number of CpGs. The relative amount of hemimethylated CpGs is the ratio between hemimethylated CpGs and total methylated CpGs. (**E**) The methylation patterns are subdivided into four groups. Unbiased hemimethylation represents clones with hemimethylated CpG sites in both strands. Biased hemimethylation represents clones with hemimethylated CpG sites in one strand. Full methylation represents methylation of all CpG sites. Non-methylation represents no methylation of any CpG sites. *P* values were obtained using χ^2 test.

Given that CpG methylation of SINEs is eventually completely erased in gonadal PGCs, SINE demethylation in migrating PGCs might be necessary for the early differentiation of PGCs during migrating periods. Interestingly, the reactivation of pluripotency-associated genes such as *Nanog*, *Klf2* and *Dppa3* occurs in PGCs at early migrating periods, soon after the specific repression of *Dnmt3b* transcription (Kurimoto et al., 2008; Yabuta et al., 2006). Generally, SINEs are extremely low in the PolII promoter region, whereas we have previously shown that SINEs are significantly enriched in the promoter region of germline-specific genes, including *Nanog*, *Klf2* and *Dppa3* (Ichiyanagi et al., 2011). We hypothesised that the erasure of DNA methylation on SINEs dispersed across genome is sufficient for the complete activation of early PGC markers in migrating PGCs. Consistent with our hypothesis, a recent study showed that CpG methylation on SINE-like sequences commonly distributed in *Ifitm1*, *Prdm1* and *Dppa3* are consistently erased in migrating PGCs (Mochizuki et al., 2012).

Specific repression of an essential factor for DNA and H3K9 methylation

Whole-mount immunofluorescence analysis was performed to determine the precise timing of the repression of essential factors for DNA and H3K9 methylation in nascent PGCs, including DNMT3A, DNMT3B, UHRF1 and GLP. Several previous studies have shown that the loss of these factors is associated with replication-dependent passive DNA demethylation (Chen et al., 2003; Dong et al., 2008; Sharif et al., 2007). Although specifying PGCs proliferate rapidly, they enter G2 cell cycle arrest between E7.75 and E9.0, after which time they resume proliferation (Seki et al., 2007). The timing of SINEs and LINE-1 DNA demethylation coincides with the active proliferation phase of PGCs. In addition, protein levels of DNMT3B and UHRF1 are gradually decreased in nascent PGCs during the first phase of PGC proliferation at E6.25-E7.5. We observed the reduction of DNA methylation on SINEs, but not on LINE-1, in *Dnmt3b* KO ESCs (N.O., K. Ebi and Y.S., unpublished data), which suggests that the dependency on DNMT3B of the maintenance of DNA methylation on SINEs is stronger than that on LINE-1 during DNA replication. Accordingly, we considered that the complete absence of DNMT3B and the slight reduction of UHRF1, coupled with the rapid proliferation of PGCs, is involved in passive DNA demethylation of SINEs, but not LINE-1, in nascent PGCs. By contrast, DNMT3A, DNMT3B, UHRF1 and GLP proteins are undetectable in gonadal PGCs during the second phase of PGC

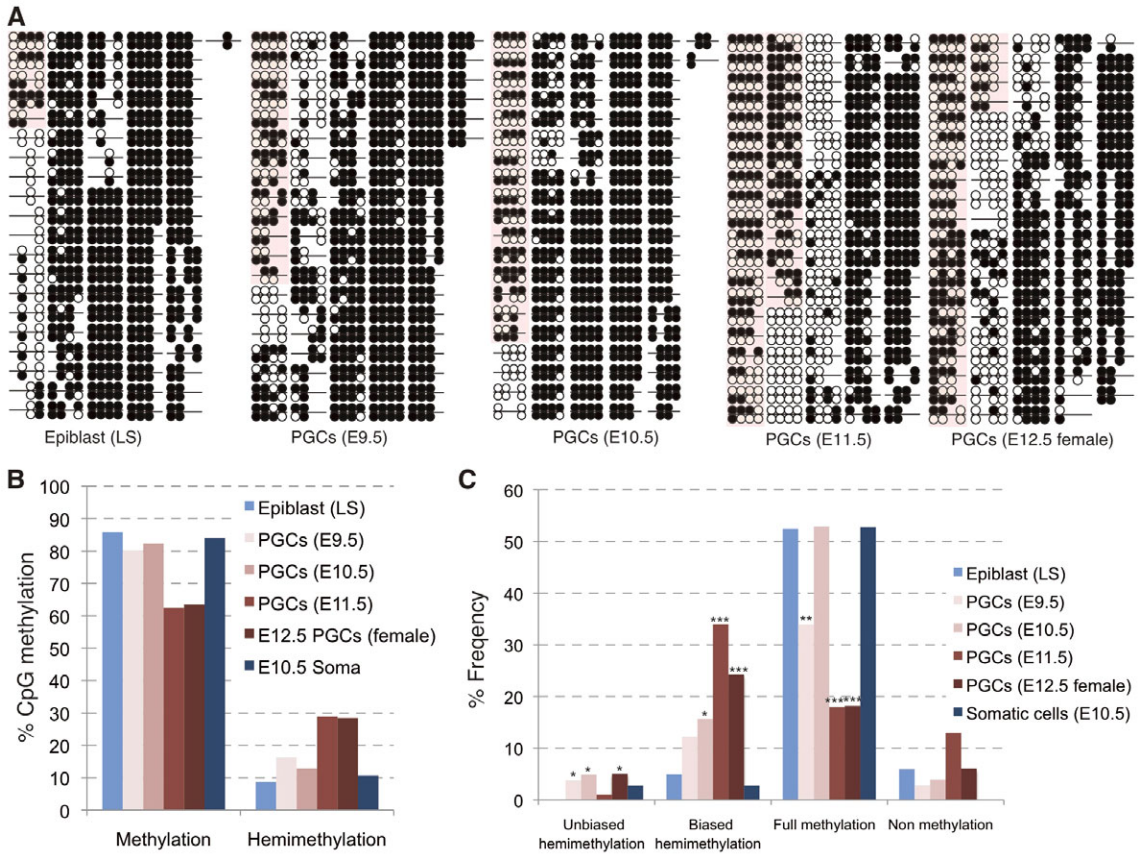

Fig. 6. Hemimethylation in LINE-1 during PGC development. (**A**) Methylation patterns, represented by circles, derived from epiblasts (E6.75) and PGCs (E9.5 to E12.5). Filled, methylated; open, unmethylated. Pink shading indicates biased hemimethylated clones. (**B**) The total amount of methylated CpGs per total CpG numbers. The relative amount of hemimethylated CpGs is the ratio between hemimethylated CpGs and total methylated CpGs. (**C**) The methylation patterns are subdivided to four groups. Unbiased hemimethylation represents clones with hemimethylated CpG sites in both strands. Biased hemimethylation represents clones with hemimethylated CpG sites in one strand. Full methylation represents methylation of all CpG sites. Non-methylation represents no methylation of any CpG sites. *P* values were obtained using χ^2 test. **P*<0.05, ***P*<0.01, ****P*<0.001.

proliferation after E9.5, which might result in the induction of passive DNA demethylation of both SINEs and LINE-1 (Fig. 7C).

H3K9 demethylation in migrating PGCs

Our ChIP analysis of developing PGCs indicated that H3K9me1/2 marks in SINEs and LINE-1 are substantially erased during their development until E9.5. Changes in H3K9 methylation in SINEs and LINE-1 in developing PGCs are similar to those in *Glp* KO ESCs, which suggests that active repression of GLP expression triggers global H3K9 demethylation in developing PGCs. G9a is an essential partner of GLP in the H3K9 methylation complex, and it is required for the maintenance in ESCs of DNA methylation in the promoter regions of germline-specific genes and the Rhox gene cluster, which are expressed in developing PGCs (Daggag et al., 2008; Dong et al., 2008; Myant et al., 2011). Considering these findings, we speculate that the repression of GLP expression establishes the primed state of transcription of germline-specific genes in developing PGCs, allowing germ cells derived from PGCs to fully activate germline-specific genes during further differentiation.

The role of PGC proliferation in DNA demethylation in PGCs

Alkaline phosphatase staining, the classical method for counting PGC numbers, indicated that the doubling time of PGCs is about 16 hours and that developing PGCs continually increase in number (Tam and Snow, 1981). By contrast, the erasure of genomic imprinting occurs at specific periods in which PGCs enter the embryonic gonad, leading us to suggest that the active mechanisms of DNA demethylation induced by the gonadal environment are involved in the erasure of genomic imprinting, which is independent of DNA replication in PGCs (Hajkova et al., 2002). However, our previous study showed that the doubling time of developing PGCs is not constant (Seki et al., 2007). Whereas nascent PGCs proliferate rapidly until E7.25, the majority of the migrating PGCs are in the G2 phase of the cell cycle, and they re-enter the proliferation phase after E9.5, which coincides with the arrival of PGCs at the genital ridges. Interestingly, G2 cell cycle arrest was also observed in primordial germ cell-like cells (PGCLCs) generated from ESCs *in vitro* (Hayashi et al., 2011), suggesting that intrinsic molecular programmes regulate G2 cell cycle arrest in migrating PGCs, and that extrinsic cues from the gonadal environment relieve the cell cycle arrest of PGCs.

The relationship between passive demethylation and active demethylation in PGCs

Hajkova et al. suggested that because the majority of PGCs exist in the G2 phase of the cell cycle, gonadal PGCs undergo global DNA demethylation without DNA replication at E11.5 (Hajkova et al.,

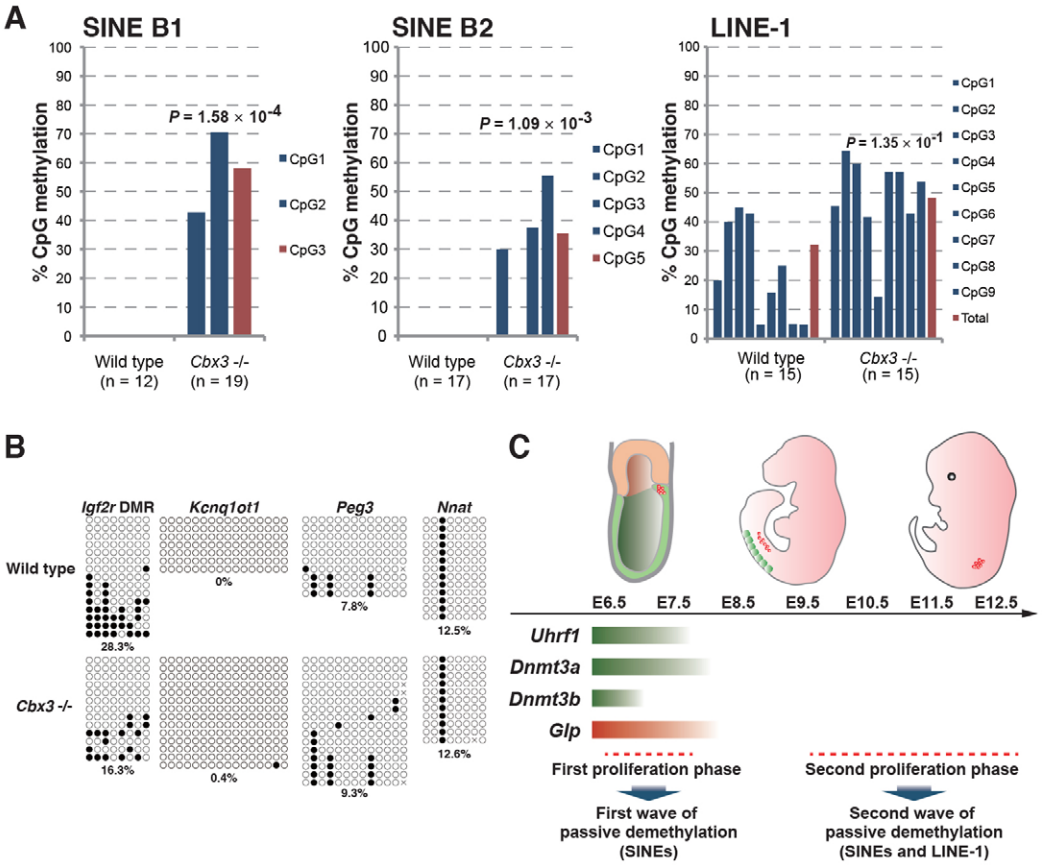

Fig. 7. DNA methylation in *Cbx3*-deficient PGCs is retained in SINEs and LINE-1 but not in imprinted regions. (**A**,**B**) Bisulphite sequencing analysis of SINEs, LINE-1 and imprinted regions in wild-type and *Cbx3*-deficient PGCs at E11.5. *P* values were obtained using the non-parametric two-tailed Mann–Whitney *U* test. In B, filled circles represent methylated and open circles represent unmethylated CpG sites. (**C**) Model of passive demethylation in PGCs during their development. Nascent PGCs begin to repress four major modifiers of DNA and histone methylation associated with rapid proliferation (first proliferation phase). Complete reduction of *Dnmt3b* expression and partial reductions of *Dnmt3a2*, *Uhrf1* and *Glp* expression coupled with rapid proliferation might induce replication-dependent passive demethylation on SINEs in nascent PGCs. The majority of migrating PGCs enter into G2 arrest from E7.75 to E9.25. Complete reduction of *Dnmt3a/b*, *Uhrf1* and *Glp* expression coupled with rapid proliferation (second proliferation phase) might modulate replication-dependent passive demethylation both on SINEs and LINE-1 in gonadal PGCs.

2008). However, we and other research groups have shown that PGCs continue to proliferate rapidly from E10.5 to E12.5, and we were unable to detect G2 cell cycle arrest in gonadal PGCs (Kagiwada et al., 2013; Western et al., 2008). Recently, we showed that replication-coupled passive DNA demethylation of genomic imprints might be induced by rapid cycling with the reduction of UHRF1 protein levels in PGCs (Kagiwada et al., 2013). In this previous study, we carefully analysed the cell cycle and localisation of DNMT1 in gonadal PGCs after E10.5. Our current study demonstrates that DNMT1 is localised at replication foci in nascent PGCs until E7.5, whereas a diffuse localisation of DNMT1 in nucleoplasm at mid-late S phase was observed in PGCs after E9.5. Furthermore, hairpin-bisulphite sequencing of LINE-1 in wild-type PGCs and DNA methylation analysis of *Cbx3*-deficient PGCs, showing severe inhibition of G1/S progression, support the existence of replication-coupled passive DNA demethylation. Seisenberger et al. also monitored hemimethylated CpG on LINE-1 by hairpin bisulphite sequencing analysis (Seisenberger et al., 2012). Our data showed the elevation of the frequency of strand-specific hemimethylated clones in PGCs from E10.5 to E11.5, and a substantial number of hemimethylated CpG sites was observed in PGCs at E9.5 and E10.5 in a recent study (Seisenberger et al., 2012). Our primer set in hairpin bisulphite sequencing amplified a shorter region of LINE-1 5′UTR than that used in the previous study. Therefore, it is possible that our primer set preferentially amplified the truncated form of LINE-1, which might have caused the differences between the two studies. The total number of cell divisions was lower in *Cbx3*-deficient PGCs than in wild-type PGCs from E7.75 to E11.5 (Abe et al., 2011). The DNA demethylation impairment in LINE-1 was consistent with the reduction in cell division in *Cbx3*-deficient PGCs. However, the severity of impairment of DNA demethylation in SINEs in *Cbx3*-deficient PGCs was high, suggesting the direct role of CBX3 in DNA demethylation on SINEs of migrating PGCs, in addition to cell cycle regulation. Further detailed studies are required to elucidate the abnormality of DNA demethylation in *Cbx3*-deficient PGCs.

Progeny derived from *Tet1*/*Tet2*-deficient mice showed increased methylation levels at differentially methylated regions (DMRs) of the imprinting locus, which might be caused by impaired erasing of genomic imprinting in *Tet1*/*Tet2*-deficient PGCs (Dawlaty et al., 2013). Furthermore, both single knockout of *Tet1* in PGCs and dual knockdown of *Tet1*/*Tet2* in PGCLCs showed that TET1 and TET2 are required for substantial DNA demethylation of germline-specific genes (Hackett et al., 2013; Yamaguchi et al., 2012). Results of the

current study as well as our previous study provide evidence that DNA demethylation in LINE-1 depends on DNA replication in the PGCs (Kagiwada et al., 2013), whereas the impairment in DNA demethylation observed in *Tet1*/*Tet2*-knockdown PGCLCs was associated with cell cycle arrest (Hackett et al., 2013). These findings suggest that both active and passive mechanisms act within the same loci, such as LINE-1, in PGCs. We considered that the impairment of DNA demethylation caused by loss of the candidate molecules for active DNA demethylation (such as *Tet1*/*Tet2* knockout) would be compensated for by passive demethylation in PGCs (Dawlaty et al., 2013). We conclude that not only the loss-of-function experiments in PGCs or PGCLCs but also the reconstitution of the molecular pathway of active DNA demethylation in epiblast-like cells (EpiLCs), which are PGC precursors, are necessary to elucidate the epigenetic network of DNA demethylation associated with PGC development.

Acknowledgements
We thank H. Koseki and J. Sharif for cell lines; H. Ohta for isolation of PGCs; Y. Shinkai for helpful comments; and all the members of our laboratory for their discussion of this study.

Funding
This study was supported in part by a Grant-in-Aid from the Ministry of Education, Culture, Sports, Science, and Technology of Japan; by the Takeda Science Foundation; by the Kwansei Gakuin personal special funding; by Chemicals Evaluation and Research Institute; and by a grant of individual special research A from Kwansei Gakuin university.

Competing interests statement
The authors declare no competing financial interests.

Author contributions
R.O. and M.N. performed immunofluorescence, hairpin-bisulphite sequencing, and bisulphite sequencing analysis. M.S. advised on the experimental design. C.N. and M.A. performed the purification of PGCs derived from *Cbx3*-deficient embryos. N.O. and O.T. performed bisulphite sequencing analysis. M.T. established *Glp* KO ESCs. Y.S. conceived and designed all experiments and performed bisulphite sequencing, ChIP, and immunofluorescence analysis, and wrote and edited the manuscript.

Supplementary material
Supplementary material available online at
http://dev.biologists.org/lookup/suppl/doi:10.1242/dev.093229/-/DC1

References
Abe, K., Naruse, C., Kato, T., Nishiuchi, T., Saitou, M. and Asano, M. (2011). Loss of heterochromatin protein 1 gamma reduces the number of primordial germ cells via impaired cell cycle progression in mice. *Biol. Reprod.* **85**, 1013-1024.
Agger, K., Cloos, P. A., Christensen, J., Pasini, D., Rose, S., Rappsilber, J., Issaeva, I., Canaani, E., Salcini, A. E. and Helin, K. (2007). UTX and JMJD3 are histone H3K27 demethylases involved in HOX gene regulation and development. *Nature* **449**, 731-734.
Arand, J., Spieler, D., Karius, T., Branco, M. R., Meilinger, D., Meissner, A., Jenuwein, T., Xu, G., Leonhardt, H., Wolf, V. et al. (2012). In vivo control of CpG and non-CpG DNA methylation by DNA methyltransferases. *PLoS Genet.* **8**, e1002750.
Bird, A. (2002). DNA methylation patterns and epigenetic memory. *Genes Dev.* **16**, 6-21.
Chen, T., Ueda, Y., Dodge, J. E., Wang, Z. and Li, E. (2003). Establishment and maintenance of genomic methylation patterns in mouse embryonic stem cells by Dnmt3a and Dnmt3b. *Mol. Cell. Biol.* **23**, 5594-5605.
Daggag, H., Svingen, T., Western, P. S., van den Bergen, J. A., McClive, P. J., Harley, V. R., Koopman, P. and Sinclair, A. H. (2008). The rhox homeobox gene family shows sexually dimorphic and dynamic expression during mouse embryonic gonad development. *Biol. Reprod.* **79**, 468-474.
Dawlaty, M. M., Breiling, A., Le, T., Raddatz, G., Barrasa, M. I., Cheng, A. W., Gao, Q., Powell, B. E., Li, Z., Xu, M. et al. (2013). Combined deficiency of Tet1 and Tet2 causes epigenetic abnormalities but is compatible with postnatal development. *Dev. Cell* **24**, 310-323.
Dong, K. B., Maksakova, I. A., Mohn, F., Leung, D., Appanah, R., Lee, S., Yang, H. W., Lam, L. L., Mager, D. L., Schübeler, D. et al. (2008). DNA methylation in ES cells requires the lysine methyltransferase G9a but not its catalytic activity. *EMBO J.* **27**, 2691-2701.
Feldman, N., Gerson, A., Fang, J., Li, E., Zhang, Y., Shinkai, Y., Cedar, H. and Bergman, Y. (2006). G9a-mediated irreversible epigenetic inactivation of Oct-3/4 during early embryogenesis. *Nat. Cell Biol.* **8**, 188-194.
Gu, T. P., Guo, F., Yang, H., Wu, H. P., Xu, G. F., Liu, W., Xie, Z. G., Shi, L., He, X., Jin, S. G. et al. (2011). The role of Tet3 DNA dioxygenase in epigenetic reprogramming by oocytes. *Nature* **477**, 606-610.
Guibert, S., Forné, T. and Weber, M. (2012). Global profiling of DNA methylation erasure in mouse primordial germ cells. *Genome Res.* **22**, 633-641.
Guo, J. U., Su, Y., Zhong, C., Ming, G. L. and Song, H. (2011). Hydroxylation of 5-methylcytosine by TET1 promotes active DNA demethylation in the adult brain. *Cell* **145**, 423-434.
Hackett, J. A., Sengupta, R., Zylicz, J. J., Murakami, K., Lee, C., Down, T. A. and Surani, M. A. (2013). Germline DNA demethylation dynamics and imprint erasure through 5-hydroxymethylcytosine. *Science* **339**, 448-452.
Hajkova, P., Erhardt, S., Lane, N., Haaf, T., El-Maarri, O., Reik, W., Walter, J. and Surani, M. A. (2002). Epigenetic reprogramming in mouse primordial germ cells. *Mech. Dev.* **117**, 15-23.
Hajkova, P., Ancelin, K., Waldmann, T., Lacoste, N., Lange, U. C., Cesari, F., Lee, C., Almouzni, G., Schneider, R. and Surani, M. A. (2008). Chromatin dynamics during epigenetic reprogramming in the mouse germ line. *Nature* **452**, 877-881.
Hajkova, P., Jeffries, S. J., Lee, C., Miller, N., Jackson, S. P. and Surani, M. A. (2010). Genome-wide reprogramming in the mouse germ line entails the base excision repair pathway. *Science* **329**, 78-82.
Hayashi, K., Ohta, H., Kurimoto, K., Aramaki, S. and Saitou, M. (2011). Reconstitution of the mouse germ cell specification pathway in culture by pluripotent stem cells. *Cell* **146**, 519-532.
He, Y. F., Li, B. Z., Li, Z., Liu, P., Wang, Y., Tang, Q., Ding, J., Jia, Y., Chen, Z., Li, L. et al. (2011). Tet-mediated formation of 5-carboxylcytosine and its excision by TDG in mammalian DNA. *Science* **333**, 1303-1307.
Ichiyanagi, K., Li, Y., Watanabe, T., Ichiyanagi, T., Fukuda, K., Kitayama, J., Yamamoto, Y., Kuramochi-Miyagawa, S., Nakano, T., Yabuta, Y. et al. (2011). Locus- and domain-dependent control of DNA methylation at mouse B1 retrotransposons during male germ cell development. *Genome Res.* **21**, 2058-2066.
Iqbal, K., Jin, S. G., Pfeifer, G. P. and Szabó, P. E. (2011). Reprogramming of the paternal genome upon fertilization involves genome-wide oxidation of 5-methylcytosine. *Proc. Natl. Acad. Sci. USA* **108**, 3642-3647.
Ito, S., Shen, L., Dai, Q., Wu, S. C., Collins, L. B., Swenberg, J. A., He, C. and Zhang, Y. (2011). Tet proteins can convert 5-methylcytosine to 5-formylcytosine and 5-carboxylcytosine. *Science* **333**, 1300-1303.
Kagiwada, S., Kurimoto, K., Hirota, T., Yamaji, M. and Saitou, M. (2013). Replication-coupled passive DNA demethylation for the erasure of genome imprints in mice. *EMBO J.* **32**, 340-353.
Kobayashi, H., Sakurai, T., Miura, F., Imai, M., Mochiduki, K., Yanagisawa, E., Sakashita, A., Wakai, T., Suzuki, Y., Ito, T. et al. (2013). High-resolution DNA methylome analysis of primordial germ cells identifies gender-specific reprogramming in mice. *Genome Res.* **23**, 616-627.
Kurimoto, K., Yabuta, Y., Ohinata, Y., Shigeta, M., Yamanaka, K. and Saitou, M. (2008). Complex genome-wide transcription dynamics orchestrated by Blimp1 for the specification of the germ cell lineage in mice. *Genes Dev.* **22**, 1617-1635.
Laird, C. D., Pleasant, N. D., Clark, A. D., Sneeden, J. L., Hassan, K. M., Manley, N. C., Vary, J. C., Jr, Morgan, T., Hansen, R. S. and Stöger, R. (2004). Hairpin-bisulfite PCR: assessing epigenetic methylation patterns on complementary strands of individual DNA molecules. *Proc. Natl. Acad. Sci. USA* **101**, 204-209.
Martens, J. H., O'Sullivan, R. J., Braunschweig, U., Opravil, S., Radolf, M., Steinlein, P. and Jenuwein, T. (2005). The profile of repeat-associated histone lysine methylation states in the mouse epigenome. *EMBO J.* **24**, 800-812.
Mochizuki, K., Tachibana, M., Saitou, M., Tokitake, Y. and Matsui, Y. (2012). Implication of DNA demethylation and bivalent histone modification for selective gene regulation in mouse primordial germ cells. *PLoS ONE* **7**, e46036.
Myant, K., Termanis, A., Sundaram, A. Y., Boe, T., Li, C., Merusi, C., Burrage, J., de Las Heras, J. I. and Stancheva, I. (2011). LSH and G9a/GLP complex are required for developmentally programmed DNA methylation. *Genome Res.* **21**, 83-94.
Ohinata, Y., Payer, B., O'Carroll, D., Ancelin, K., Ono, Y., Sano, M., Barton, S. C., Obukhanych, T., Nussenzweig, M., Tarakhovsky, A. et al. (2005). Blimp1 is a critical determinant of the germ cell lineage in mice. *Nature* **436**, 207-213.
Payer, B., Chuva de Sousa Lopes, S. M., Barton, S. C., Lee, C., Saitou, M. and Surani, M. A. (2006). Generation of stella-GFP transgenic mice: a novel tool to study germ cell development. *Genesis* **44**, 75-83.
Peters, A. H. and Schübeler, D. (2005). Methylation of histones: playing memory with DNA. *Curr. Opin. Cell Biol.* **17**, 230-238.
Popp, C., Dean, W., Feng, S., Cokus, S. J., Andrews, S., Pellegrini, M., Jacobsen, S. E. and Reik, W. (2010). Genome-wide erasure of DNA

methylation in mouse primordial germ cells is affected by AID deficiency. *Nature* **463**, 1101-1105.
Saitou, M., Kagiwada, S. and Kurimoto, K. (2012). Epigenetic reprogramming in mouse pre-implantation development and primordial germ cells. *Development* **139**, 15-31.
Sasaki, H. and Matsui, Y. (2008). Epigenetic events in mammalian germ-cell development: reprogramming and beyond. *Nat. Rev. Genet.* **9**, 129-140.
Seisenberger, S., Andrews, S., Krueger, F., Arand, J., Walter, J., Santos, F., Popp, C., Thienpont, B., Dean, W. and Reik, W. (2012). The dynamics of genome-wide DNA methylation reprogramming in mouse primordial germ cells. *Mol. Cell* **48**, 849-862.
Seki, Y., Hayashi, K., Itoh, K., Mizugaki, M., Saitou, M. and Matsui, Y. (2005). Extensive and orderly reprogramming of genome-wide chromatin modifications associated with specification and early development of germ cells in mice. *Dev. Biol.* **278**, 440-458.
Seki, Y., Yamaji, M., Yabuta, Y., Sano, M., Shigeta, M., Matsui, Y., Saga, Y., Tachibana, M., Shinkai, Y. and Saitou, M. (2007). Cellular dynamics associated with the genome-wide epigenetic reprogramming in migrating primordial germ cells in mice. *Development* **134**, 2627-2638.
Sharif, J., Muto, M., Takebayashi, S., Suetake, I., Iwamatsu, A., Endo, T. A., Shinga, J., Mizutani-Koseki, Y., Toyoda, T., Okamura, K. et al. (2007). The SRA protein Np95 mediates epigenetic inheritance by recruiting Dnmt1 to methylated DNA. *Nature* **450**, 908-912.
Tachibana, M., Sugimoto, K., Nozaki, M., Ueda, J., Ohta, T., Ohki, M., Fukuda, M., Takeda, N., Niida, H., Kato, H. et al. (2002). G9a histone methyltransferase plays a dominant role in euchromatic histone H3 lysine 9 methylation and is essential for early embryogenesis. *Genes Dev.* **16**, 1779-1791.
Tachibana, M., Matsumura, Y., Fukuda, M., Kimura, H. and Shinkai, Y. (2008). G9a/GLP complexes independently mediate H3K9 and DNA methylation to silence transcription. *EMBO J.* **27**, 2681-2690.
Tam, P. P. and Snow, M. H. (1981). Proliferation and migration of primordial germ cells during compensatory growth in mouse embryos. *J. Embryol. Exp. Morphol.* **64**, 133-147.
Western, P. S., Miles, D. C., van den Bergen, J. A., Burton, M. and Sinclair, A. H. (2008). Dynamic regulation of mitotic arrest in fetal male germ cells. *Stem Cells* **26**, 339-347.
Wossidlo, M., Nakamura, T., Lepikhov, K., Marques, C. J., Zakhartchenko, V., Boiani, M., Arand, J., Nakano, T., Reik, W. and Walter, J. (2011). 5-Hydroxymethylcytosine in the mammalian zygote is linked with epigenetic reprogramming. *Nat. Commun.* **2**, 241.
Wu, S. C. and Zhang, Y. (2010). Active DNA demethylation: many roads lead to Rome. *Nat. Rev. Mol. Cell Biol.* **11**, 607-620.
Yabuta, Y., Kurimoto, K., Ohinata, Y., Seki, Y. and Saitou, M. (2006). Gene expression dynamics during germline specification in mice identified by quantitative single-cell gene expression profiling. *Biol. Reprod.* **75**, 705-716.
Yamaguchi, S., Hong, K., Liu, R., Shen, L., Inoue, A., Diep, D., Zhang, K. and Zhang, Y. (2012). Tet1 controls meiosis by regulating meiotic gene expression. *Nature* **492**, 443-447.
Yamaji, M., Seki, Y., Kurimoto, K., Yabuta, Y., Yuasa, M., Shigeta, M., Yamanaka, K., Ohinata, Y. and Saitou, M. (2008). Critical function of Prdm14 for the establishment of the germ cell lineage in mice. *Nat. Genet.* **40**, 1016-1022.
Zhu, J. K. (2009). Active DNA demethylation mediated by DNA glycosylases. *Annu. Rev. Genet.* **43**, 143-166.

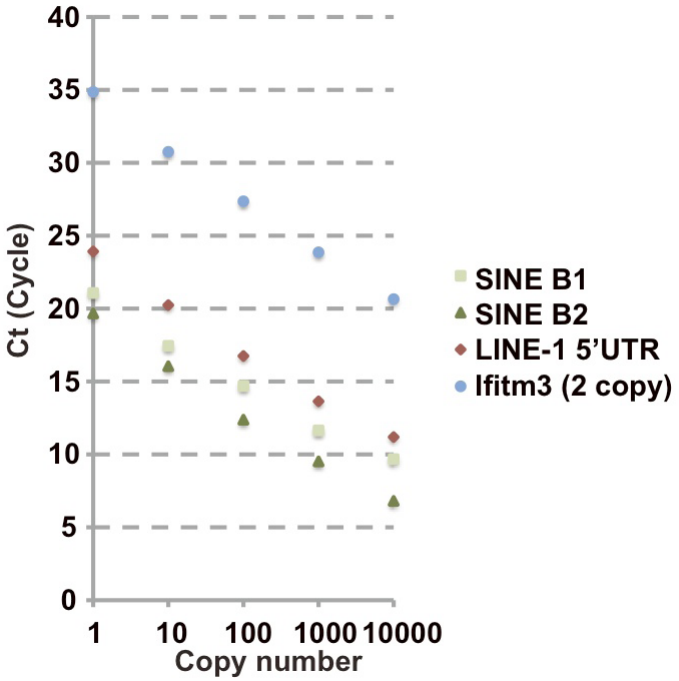

Fig. S1. Estimate of the copy number of transposable elements. Primer efficiency of ChIP against *Ifitm3* (single copy gene), SINE B1, B2 and LINE-1. Ct values of *Ifitm3* derived from 1000 to 10,000 copies of genomic DNA is almost equivalent to Ct values of SINEs B1, B2, and LINE-1 derived from 1 copy of genomic DNA.

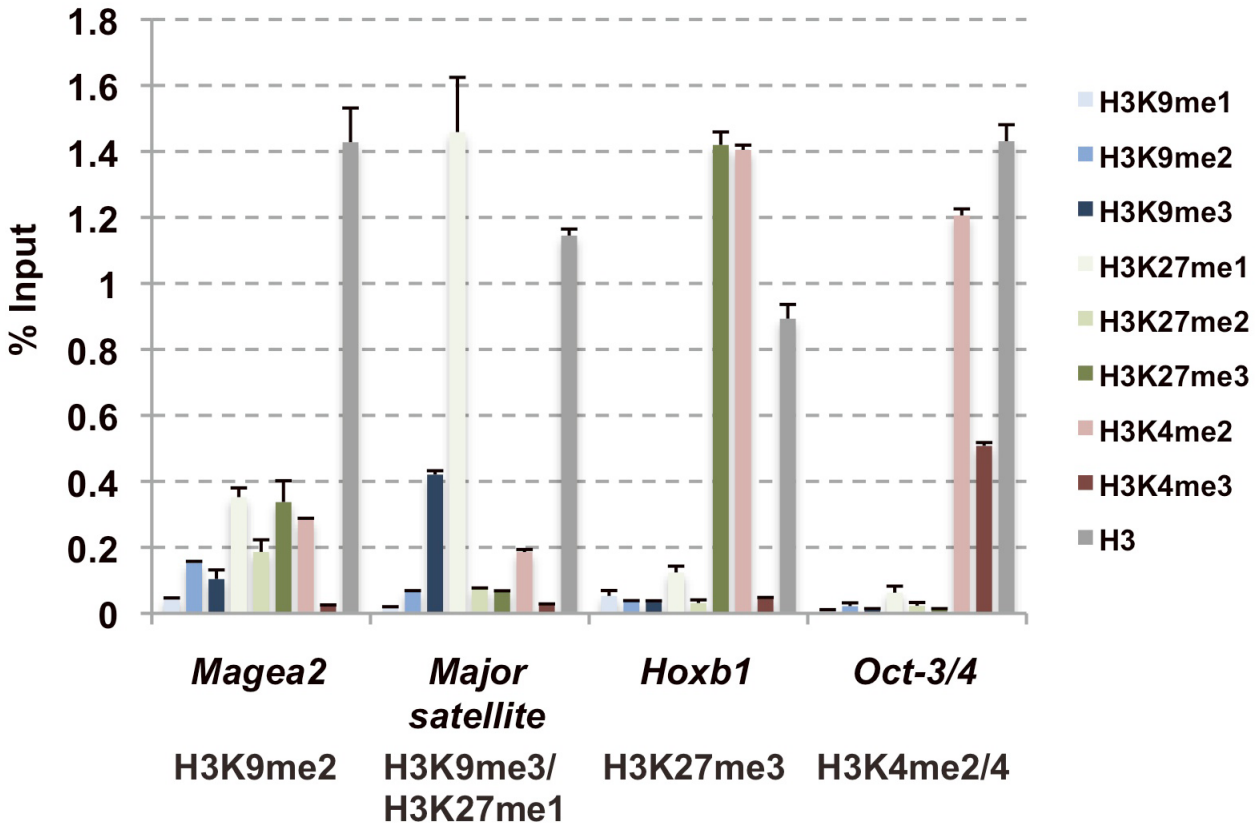

Fig. S2. Control ChIP experiments in ESCs. ChIP-PCR analysis with anti-H3K9me1/2/3, -H3K27me1/2/3, -H3K4me2/3 and -H3 antibodies in ESCs. The *y*-axis shows percent of input recovery; error bars represent s.e.m. from two technical replicates of qPCR.

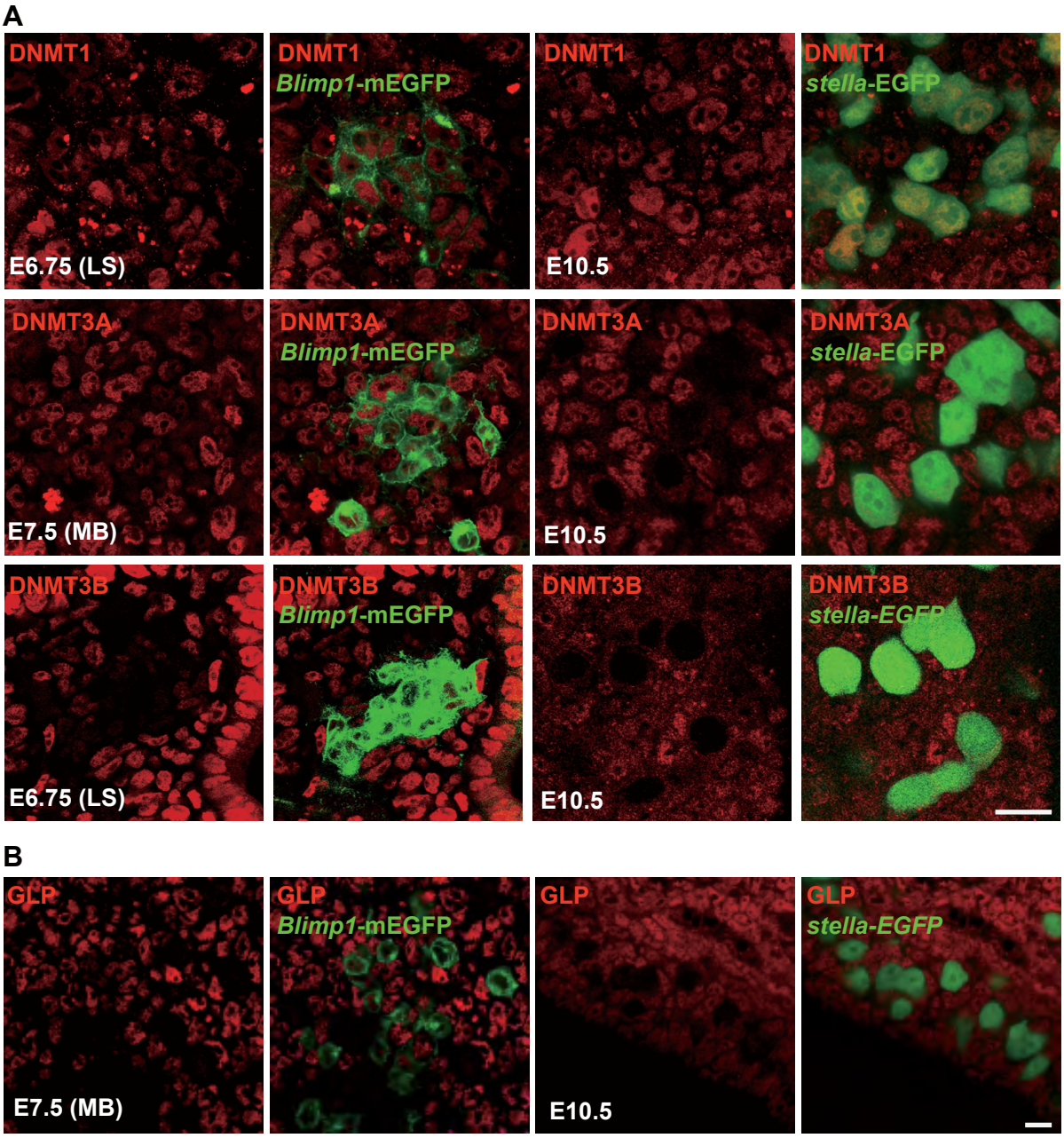

Fig. S3. Expression of DNMT1, DNMT3A/B and GLP in PGCs. (**A**,**B**) Whole-mount immunofluorescence analysis of *Prdm1*-EGFP and *Dppa3*-EGFP transgenic embryos with anti-EGFP, -DNMT1, -DNMT3A/B and -GLP antibodies. Arrowheads indicate EGFP-positive PGCs. Scale bar: 10 μm.

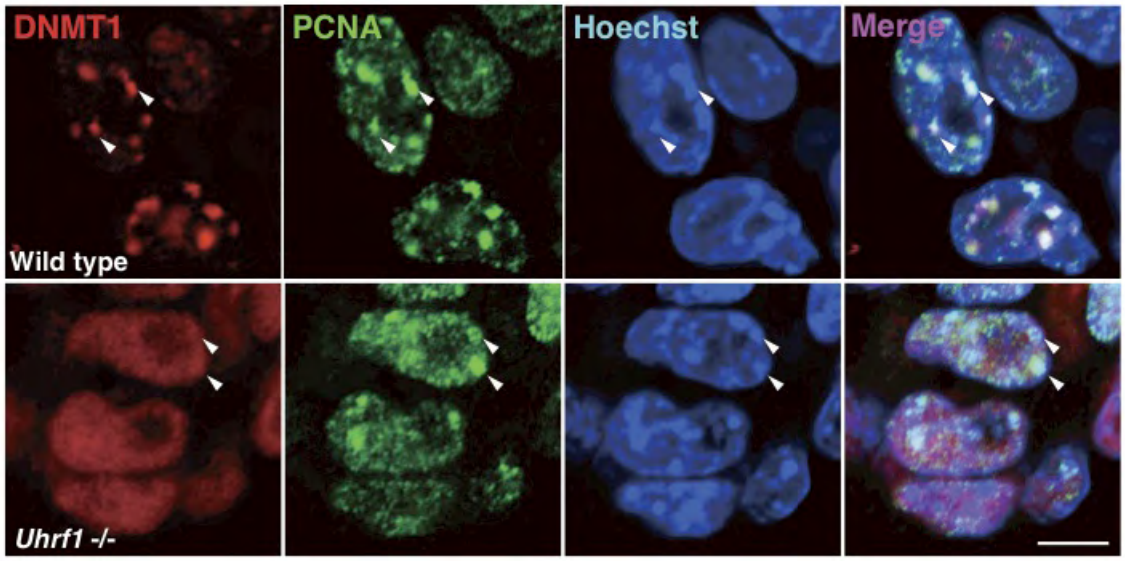

Fig. S4. Nuclear distribution of DNMT1 at the middle of S phase of cell cycle in wild-type and *Uhrf1*$^{-/-}$ ESCs. Immunofluorescence analysis of wild-type and *Uhrf1*$^{-/-}$ ESCs with anti-DNMT1 (red) and -PCNA (green) antibodies. Arrowheads indicate the replication foci at the middle of S phase of cell cycle. Scale bar: 10 μm.

Table S1. Primer sequences for bisulphite sequencing, ChIP and qRT-PCR

Bisulphite sequence

Gene	Strand	Sequence (5′-3′)
SINE B1	F	GTTTTTAATTTTAGTATTTG
	R	ATTTCTCTATATAACCCTAACTATCC
SINE B1_Mus2	F	TGGTGGTGGTGGTTGAGATAG
	R	CACACACCTTTAATCCCAACACTC
SINE B2	F	GGTTGGTGAGATGGTTTAGTGG
	R	CACTATAACTATCTTCAAACACTCC
LINE-1	F	TAGGAAATTAGTTTGAATAGGTGAGAGGT
	R	CCAAAACAAAACCTTTCTFAAACACTATAT
Peg3	F	AATAAATGAGAGAGAAAGAAAGAGAG
	R	CCAACCTAAAATACCAAATAAAAAC
Nnat 1st	F	ATTTTTTTTATATTTTTTTTAGAGTAG
	R	ACCTTTTTTCTACATTCCTACTA
Nnat 2nd	F	TTTTTTTAGAGTAGATATAATTG
	R	TTTTTCTACATTCCTACTAATCC
Kcnq1ot1 1st	F	GGTTTAGTTAGGAAGGGATG
	R	CTAACTAATATAACCTCACC
Kcnq1ot1 2nd	F	TTTGGTTAATAAAAATAGTTAGT
	R	CAAAAAAAAACACACTAAAATA
Igf2r 1st	F	TTGGATAGTGTAGAGTTTTT
	R	TAATTCTAATTATACCAAATT
Igf2r 2nd	F	TTAGTGGGGTATTTTTATTTGTATGG
	R	AAATATCCTAAAAATACAAACTACACAA

ChIP

Gene	Strand	Sequence (5′-3′)
SINE B1	F	GGTGTGGTGGCGCACACC
	R	CCTGGCTGTCCTGGAGCTC
SINE B2	F	GATGGCTCAGTGGGTAAGAGC
	R	CACTATAACTATCTTCAAACACTCC
LINE-1	F	CCAAAGCAACACAGTGTCTGAG
	R	TGCTGGCAAGCTCTCTTACAG
Magea2	F	GGACTCTGCGCCATTTTGTTCTGG
	R	GCTAGGCAGGCTAAAGGTTGACC
Major satellite	F	GACGACTTGAAAAATGACGAAATC
	R	CATATTCCAGGTCCTTCAGTGTGC
Hoxb1	F	GCCATGGGCTCAAGCTTCAGC
	R	GTCCATGTAGAGGCCGAAGGAG
Oct-3/4	F	CTGACCCTAGCCAACAGCTC
	R	TGCTCCTACACCATGCTCTG

qRT-PCR

Gene	Strand	Sequence (5′-3')
SINE B1	F	GGTGTGGTGGCGCACACC
	R	CCTGGCTGTCCTGGAGCTC
SINE B2	F	GATGGCTCAGTGGGTAAGAGC
	R	CACTATAACTATCTTCAAACACTCC
LINE-1	F	GGGATCTTCAACCCTATAGGTGGAAC

	R	TCTGCGTGTCCAATGGGCCTC

Hairpin bisulphite sequencing

Hairpin linker		AGCGATGCGTTCGAGCATCGCTCCGG
PCR primer 1st	F	GTATAGAGGGGTTGAGGTAGTATTTTG
	R	CCTAACAACTTCTAAAACAAACAAAAACAC
PCR primer 2nd	F	AGGGGTTGAGGTAGTATTTT
	R	AAAACACAAAAAAACTAAAAC